IEEE Access
Multidisciplinary | Rapid Review | Open Access Journal

Received December 26, 2018, accepted January 19, 2019, date of publication January 24, 2019, date of current version February 14, 2019.

Digital Object Identifier 10.1109/ACCESS.2019.2894961

A Modified NSGA-II for Solving Control Allocation Optimization Problem in Lateral Flight Control System for Large Aircraft

QI BIAN[1], BRETT NENER[2], AND XINMIN WANG[1]
[1]School of Automation, Northwestern Polytechnical University, Xi'an 710129, China
[2]Department of Electrical, Electronic, and Computer Engineering, The University of Western Australia, Perth, WA 6009, Australia

Corresponding author: Qi Bian (bianqi@mail.nwpu.edu.cn)

This work was supported by the China Scholar Council under Grant 201606290105.

ABSTRACT Coordinated aileron and rudder control is crucial to the lateral control stability augmentation of an aircraft. In this paper, a modified non-dominated sorting genetic algorithm II is proposed to not only optimize the control allocation between the aileron and rudder channels on different flying quality levels but also explore the relationships between the optimum solutions and the state variables of the aircraft. In doing so, a digital, nets-based stratification method is used to initialize the search chromosomes more evenly. To improve the search efficiency of the algorithm, crowding-distance-based interpolation and elimination strategies are developed to approach the optimum Pareto frontier as close as possible. Moreover, a dynamic depth search method is proposed to balance between the global and local explorations. Finally, the control allocation relationships between the aileron and rudder channels on different flying quality levels are illustrated. The comparative simulations on a six-degree-of-freedom Boeing 747 model are carried out to verify the feasibility of the proposed algorithm.

INDEX TERMS MNSGA-II, control allocation optimization, flight control system.

I. INTRODUCTION

Large transport aircraft are inevitably affected by various turbulence events during the long distance flight. The lateral Flight Control System (FCS) is required to alleviate the adverse effects from these events as much as possible [1], [2]. The lateral FCS consists mainly of two parts: the aileron based roll control channel and the rudder based yaw control channel. Measured by vertical gyroscopes, the roll rate signal is fed back into the roll augmentation loop to keep the aircraft level; the yaw rate signal from the yaw gyroscopes is fed back into both the aileron and rudder channels to modify the yaw control [3]–[5]. Since there exists tight aerodynamic couplings between these two channels, study of the control allocation relationship between the two control surfaces, aileron and rudder, is necessary in the lateral FCS design process. Moreover, depending on mission needs and requirements, the aircraft flying qualities are classified into three levels (1-3). A lateral FCS can only perform well if it can satisfy the corresponding flying quality requirements. Thus, to design a satisfactory lateral FCS, it is necessary to study the constrained lateral control allocation optimization problem under different flying quality requirements, and explore the hidden relationships between optimal solutions and different state variables of the aircraft.

Taking advantage of the fast search strategies and the need for little prior knowledge, heuristic methods are considered as power tools dealing with a wide range of black-box optimization problems [6]. In recent years, many heuristic optimization methods have been successfully applied in aerospace engineering fields. Girish [7] proposed a hybrid particle swarm optimization local-search algorithm to solve the aircraft landing problem in a short computational time. Roy and Peyada [8] studied a novel method based on hybrid neuro-fuzzy and artificial bee colony concepts for aerodynamic parameter estimation of aircraft. Marinakis *et al.* [9] presented a hybridized algorithm of particle swarm optimization with variable neighborhood search to solve the constrained shortest path optimization problem. Nieto *et al.* [10] described a hybrid particle swarm optimization and support vector machine based model for predicting the remaining

useful life of aircraft engines. By converting the parameter design problem to an optimization problem, Deng *et al.* [11] developed a pigeon-inspired optimization algorithm to overcome difficulties in the manual parameter adjustment task. Moreover, Dou *et al.* [12] conducted a design of the automatic carrier landing system via the Levy-flight based pigeon-inspired optimization algorithm.

In this study, a Modified Non-dominated Sorting Genetic Algorithm II (MNSGA-II) is developed to discover the hidden relationships between the two control surfaces, the aileron and rudder, on different flying quality levels, and to explore the corresponding relationships between the optimum solutions and the state variables of the aircraft. To improve the search efficiency of the algorithm, a digital nets-based stratification method is implemented to evenly partition the search space and allocate the search chromosomes. A crowding-distance based interpolation strategy is developed to assign new chromosomes to the potential solution areas to find more feasible solutions. An elimination strategy is also developed to remove chromosomes in crowded areas to save computation time. Thus, not only the search ability of the algorithm is enhanced, but also the computational efficiency of the algorithm is improved. Moreover, in the optimization process, a dynamic depth search strategy is proposed to adjust the search scope in a timely manner and explore the newly discovered solution domain by reallocating the chromosome positions. Finally, the control allocation relationships on different flying quality levels are analysed and a range of simulations on the 6DoF Boeing 747 model are carried out to demonstrate the effectiveness of the proposed method over other heuristics based multi-objective optimization algorithms, namely ISFLA [25], MOVPSO [26] and HNDS [27].

In the remainder of the paper, the lateral FCS of the Boeing 747 is built in Section 2; the proposed MNSGA-II for control allocation optimization is introduced in Section 3; comparative simulations and analyses are carried out in Section 4; and the final conclusions are discussed in Section 5.

II. LATERAL FLIGHT CONTROL SYSTEM OF THE BOEING 747

A. THE 6DoF RIGID MODEL OF THE BOEING 747

Based on the hypothesis that an aircraft is a rigid body with symmetrical geometry, mass and aerodynamic characteristics, in this paper, the 6DoF rigid model of the Boeing 747 taken from [13]–[15] is written in the form of kinematic and dynamic equations as follows.

$$\begin{bmatrix}\dot{x}\\ \dot{y}\\ \dot{z}\end{bmatrix}=\begin{bmatrix}1 & 0 & 0\\ 0 & \cos\phi & -\sin\phi\\ 0 & -\sin\phi & \cos\phi\end{bmatrix}\begin{bmatrix}\cos\theta & 0 & \sin\theta\\ 0 & 1 & 0\\ -\sin\theta & 0 & \cos\theta\end{bmatrix}\times\begin{bmatrix}\cos\psi & -\sin\psi & 0\\ \sin\psi & \cos\psi & 0\\ 0 & 0 & 1\end{bmatrix}\begin{bmatrix}u\\ v\\ w\end{bmatrix} \tag{1}$$

$$\begin{bmatrix}\dot{\phi}\\ \dot{\theta}\\ \dot{\psi}\end{bmatrix}=\begin{bmatrix}1 & \sin\phi\tan\theta & \cos\phi\tan\theta\\ 0 & \cos\phi & -\sin\phi\\ 0 & -\sin\phi\sec\theta & \cos\phi\sec\theta\end{bmatrix}\begin{bmatrix}p\\ q\\ r\end{bmatrix} \tag{2}$$

$$\begin{cases}\dot{p}I_{xx}-\dot{q}I_{xy}-\dot{r}I_{xz}=\bar{q}SbC_l+qr(I_{yy}-I_{zz})\\ \qquad+(q^2-r^2)I_{yz}+pqI_{xz}-prI_{xy}\\ \dot{q}I_{yy}-\dot{r}I_{yz}-\dot{p}I_{xy}=\bar{q}ScC_m+pr(I_{zz}-I_{xx})\\ \qquad+(r^2-p^2)I_{xz}+qrI_{xy}-pqI_{yz}\\ \dot{r}I_{zz}-\dot{p}I_{xz}-\dot{q}I_{yz}=\bar{q}SbC_n+qr(I_{xx}-I_{yy})\\ \qquad+(p^2-q^2)I_{xy}+prI_{yz}-qrI_{xz}\end{cases} \tag{3}$$

$$\begin{cases}\dot{\alpha}=-\dfrac{\bar{q}Sc}{mV\cos\beta}C_N\cos\alpha+q-\tan\beta(p\cos\alpha+r\sin\alpha)\\ \qquad+\dfrac{g}{V\cos\beta}(\cos\phi\cos\theta\cos\alpha+\sin\theta\sin\alpha-\dfrac{T}{mg}\sin\alpha)\\ \dot{\beta}=\dfrac{\bar{q}S}{mV}C_Y+p\sin\alpha-r\cos\alpha+\sin\phi\cos\theta\cos\beta\\ \qquad-\dfrac{g\sin\beta}{V}(\cos\theta\cos\phi\sin\alpha-\sin\theta\cos\alpha-\dfrac{T}{mg}\cos\alpha)\\ \dot{V}=\dfrac{1}{m}(T\cos\alpha\cos\beta-\bar{q}SC_D-mg\sin\gamma)\end{cases} \tag{4}$$

where $(x, y, z)^{\mathrm{T}}$ and $(\phi, \theta, \psi)^{\mathrm{T}}$ are the position and Euler angles of the aircraft, respectively; $(u, v, w)^{\mathrm{T}}$ and $(p, q, r)^{\mathrm{T}}$ are the three-axes of the aircraft velocity and the angular rates, respectively; $(V, T, \alpha, \beta)^{\mathrm{T}}$ are the airspeed, thrust, angle of attack and sideslip angle, respectively; $(C_m, C_l, C_n)^{\mathrm{T}}$ and $(C_N, C_Y, C_D)^{\mathrm{T}}$ are the moment and force coefficients, respectively; $(I_{xx}, I_{yy}, I_{zz})^{\mathrm{T}}$ and $(I_{xy}, I_{yz}, I_{xz})^{\mathrm{T}}$ are the moments of inertia and the cross products of inertia, respectively; $(c, b, S, m, \bar{q})^{\mathrm{T}}$ are the aircraft geometries, mass and dynamic pressure. The aerodynamic parameter values of the Boeing 747 model used in this paper are defined in [15], of which all data refer to the aircraft in level flight at an altitude of 40 kft and 0.8 Mach.

The lateral wind disturbance model used in this paper is derived from [16]. By adding turbulence to the Dryden spectral model and passing band-limited white noise through a forming filter with characteristic power spectral density, the filtered signal is used as an external wind disturbance in the simulation. The lateral spectral function and its realised transfer function are presented as follows.

$$\Phi_v(\Omega)=\sigma_v^2\frac{2L}{\pi}\frac{1+12(L\Omega)^2}{[1+4(L\Omega)^2]^2} \tag{5}$$

$$G_v(s)=\sigma_v\sqrt{\frac{2L}{\pi V}}\frac{1+\frac{2\sqrt{3}L}{V}s}{(1+\frac{2L}{V}s)^2} \tag{6}$$

where V and L represent the turbulence scale length and airspeed, respectively. σ_v^2 is used to set the turbulence intensity.

B. THE LATERAL FLIGHT CONTROL SYSTEM OF THE BOEING 747

For most conventional aircraft, the lateral FCS is achieved through coordinated control of both aileron and rudder channels [17], [18]. To alleviate the yaw rate deviation that comes from the Dutch-roll mode, the rudder control channel needs

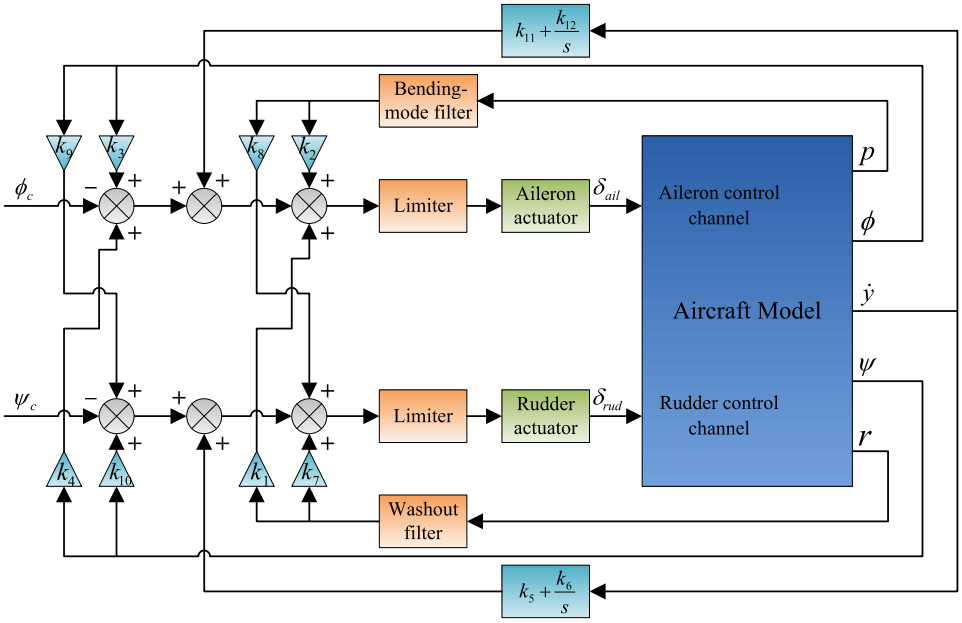

FIGURE 1. Lateral FCS structure of the Boeing 747.

to create an opposite yawing moment. The aileron control is used to reduce the variation in the roll performance under different flight conditions. The research-oriented lateral FCS structure of the Boeing 747 is shown in Fig. 1.

As shown in Fig. 1, the aileron and rudder control channels are fully coupled with each other. In order to make explicit relationships between the state variables and control surfaces, both control channel commands, δ_{ail} and δ_{rud}, are generated by integrating the weighted feedback signals of p, r, ϕ, ψ and $\dot{y}$. When an aircraft deviates from its original flight path as a result of the wind disturbance, the lateral FCS generates an aileron control command to roll the aircraft to a certain angle. Thus, the horizontal component of the lift will force the aircraft to turn in the opposite direction to offset the deviation. Simultaneously, the coordinated control of the rudder channel is applied to minimize the sideslip angle and improve the ride quality. The bending-mode filter is used to reduce the adverse effect of moments generated by ailerons sensed by the roll rate gyro. A washout filter is applied to ensure that the spiral mode of the system does not move further into the left-half plane of the complex plane and hence maintain stability. $1/s$ represents the integral operator. ϕ_c and ψ_c are the corresponding two control channel commands. $k_1 - k_{12}$ are the control gains which need to be optimized.

III. THE MODIFIED NON-DOMINATED SORTING GENETIC ALGORITHM II BASED CONTROL ALLOCATION OPTIMIZATION

A. PROBLEM FORMULATION

The flight phase studied in this paper mainly focuses on large, heavy airplanes in non-terminal flight using gradual maneuvers without precise tracking but need accurate flight-path control. In order to design a well qualified FCS, several important flight criteria, including the stability, manoeuvrability, ride quality and so on, should be considered [19]. Moreover, considering the coordinated control efficiency, engineers always want to find solutions that can not only satisfy the flying quality requirements but also cost the minimum amount of control energy. Thus, on one hand, the control energy cost relationship between the ailerons and rudder channels should be calculated; on the other hand, the relationships between the optimum solutions and the state variables of the aircraft should also be analysed. The control allocation optimization problem is formulated as follows.

$$\begin{cases} S = \min\{J_1(k), J_2(k)\} \quad s.t.\, J_3(k) = 0 \\ J_1 = \int (\delta_{ail})^2 dt \\ J_2 = \int (\delta_{rud})^2 dt \end{cases} \tag{7}$$

where S represents the solution set of control gain k. J_1 and J_2 represent the control energy costs of the ailerons and rudder channels, respectively. Besides, the quantified flying quality evaluation function J_3 to ensure all non-dominated solutions satisfy their corresponding flying quality requirements is described in the following, where J_{31} and J_{32} refer to the time constants in roll and spiral modes, respectively. J_{33} is used to evaluate the performance of the Dutch-roll mode. J_{34} represents the predefined limitations of each lateral state variable in flight phase. ω_{3i} $(i = 1, 2, 3, 4)$ represent the corresponding weight factors. t_r and t_s represent the roll mode time and the spiral mode doubling time, respectively. ξ_d and ω_d represent the damping ratio and the natural frequency of the Dutch-roll mode, respectively. Finally, the objective is to find a set of optimum non-dominated control allocation solutions of J_1 and J_2 under the condition that J_3 is satisfied. The specifications of the lateral flying quality levels are given in Table 1. The limitations of the state variables of the lateral

TABLE 1. Lateral flying quality specifications.

Flying quality levels	1	2	3
Maximum (Max.) t_r	1.4	3.0	10
Minimum (Min.) t_s	20	8	4
Min. ξ_d	0.08	0.02	0.02
Min. $\xi_d\omega_d$	0.15	0.05	no limit
Min. ω_d	0.4	0.4	0.04

TABLE 2. Limitations of lateral state variables in the MKS units.

Variable	Limitation	Variable	Limitation
r	3	p	5
ϕ	5	ψ	3
y	2	n_y	1

FCS are given in Table 2.

$$\begin{cases} J_3 = \omega_{31}J_{31}+\omega_{32}J_{32}+\omega_{33}J_{33}+\omega_{34}J_{34} \\ J_{31} = \begin{cases} 0 \ if \ t_r \ meets \ the \ specifications \\ t_r \ else \end{cases} \\ J_{32} = \begin{cases} 0 \ if \ t_s \ meets \ the \ specifications \\ 1/t_s \ else \end{cases} \\ J_{33} = \begin{cases} 0 \ if \ \xi_d \ and \ \omega_d \ meet \ the \ specifications \\ 1/\xi_d+1/\omega_d+1/(\xi_d+\omega_d) else \end{cases} \\ J_{34} = \begin{cases} 0 \ if \ all \ state \ varibles \ meet \ the \ specifications \\ \int r^2+p^2+\psi^2+\psi^2+y^2+n_y^2 \ else \end{cases} \end{cases} \tag{8}$$

B. THE MODIFIED NON-DOMINATED SORTING GENETIC ALGORITHM II

By mimicking natural evolutionary strategies to formulate the chromosomes' updating procedure, the genetic algorithm based optimization strategy and its variations have been utilized widely in many fields including engineering, mathematics, computer science, and finance [20], [21]. In this paper, a MNSGA-II is proposed to find the control allocation relationship between the aileron and rudder channels, and illuminate the characteristics of the corresponding state variables. The MNSGA-II works as follows:

Step 1: In order to improve the search efficiency of the algorithm and explore the problem domain more uniformly, the digital nets-based Quasi-Monte Carlo sampling method [22] is adopted to create the initial search group C ($C = c_1, c_2, ...c_N$) in the following ways.

$$\begin{cases} c_i = (c_{i,1}, c_{i,2}, ..., c_{i,D})^{\mathrm{T}} \\ c_{i,j} = \dfrac{y_{i,j,1}}{b} + \dfrac{y_{i,j,2}}{b^2} + ... + \dfrac{y_{i,j,m}}{b^m} \\ y_{i,j} = (y_{i,j,1}, ..., y_{i,j,m})^{\mathrm{T}} \\ n = (n_0, n_1, ..., n_m)^{\mathrm{T}} \end{cases} \tag{9}$$

where N and D represent the chromosomes' number and dimension, respectively. $c_i \in P$, and $c_{i,j}$ represents the j-th dimension of c_i. $Z_b = \{0, 1, ..., b-1\}$ is a finite field with order b, a prime number. Thus, a series of the c_i can be created according to Eq. (9), where each $c_{i,j}$ represents the j-th control gain of the i-th solution.

Step 2: Since all of the chromosomes have been assigned their corresponding control gain values, all solutions are tested in the flight simulation and the cost values (J_1, J_2 and J_3) are calculated using Eq. (8). Then the chromosomes are sorted in ascending order according to their own cost values, J_3 . Then the chromosomes with non-zero J_3 are sorted in ascending order and saved in the set C_1. For the chromosomes that satisfy the predefined flying qualities (which means $J_3 = 0$), directly pick the chromosomes on the front frontier with lower densities to generate C_2. Both C_1 and C_2 are used to generate the parent group $C_p = \{C_1, C_2\}$. A tournament selection operator [23] is used to pick the elite chromosomes from C_p. Then the offspring group C_f is generated from these elite chromosomes using the adaptive crossover and mutation operators [24]. Thus a new search group C_s can be created by sorting the chromosomes in $\{C_p, C_f\}$ according to their non-domination ranks and crowding-distances.

Step 3: In the search process, on one hand, the sparse density of chromosomes in some areas may affect the local search efficiency of the algorithm; on the other hand, the chromosomes in some areas are so crowded that the computational time is greatly increased. Thus, to improve the search efficiency and reduce computational time of the algorithm, crowding-distance based interpolation and elimination strategies are defined in the following ways: (1) Calculate the Euclidean distance d_i between the i-th chromosome c_i and its closest neighbor c_j ($c_i, c_j \in C_s$) in ascending order; (2) If $d_i > d_c$, divide the line between the two points c_i and c_j into $f_r(\frac{d_i}{d_c})$ equal parts and randomly create a new chromosome on each part, where f_r means the rounding-to-zero operation; (3) If $d_i < d_e$, directly eliminate c_j. Then check the next closest c_{j+1} until $d_i > d_e$; (4) Re-sort the chromosomes in C_s according to their crowding-distances and non-domination ranks.

Step 4: After each iteration, the search scope of the algorithm should be adjusted so that the chromosomes can exist in a more precise solution domain in the next iteration. To balance between the global and local exploration, a dynamic deepening search strategy is proposed as follows:

$$\begin{cases} L_u^{t+1} = \begin{cases} max(C_s, L_u^t) + L_0, & if \ J_3 \neq 0 \\ max(C_s, L_u^t) + \omega_d \bar{d}, & else \end{cases} \\ L_l^{t+1} = \begin{cases} min(C_s, L_u^t) - L_0, & if \ J_3 \neq 0 \\ min(C_s, L_u^t) - \omega_d \bar{d}, & else \end{cases} \\ \omega_d = \dfrac{\omega_i}{\omega_0^{t/100} + \omega_e} \end{cases} \tag{10}$$

where L_u^t and L_l^t represent upper and lower boundaries in the t-th iteration, respectively. When the algorithm is in the convergence process ($J_3 \neq 0$), a predefined L_0 is used to modify the boundaries for global exploration. When the algorithm converges, an average crowding-distance $\bar{d}$ is used to self-adjust the search scope of the algorithm, where ω_d is a weight factor controlled by ω_i, ω_0 and ω_e. Moreover, by using Eq. (9), a random re-allocation operation of the chromosomes

will be triggered after every I_r iterations in order to avoid chromosomes being trapped in local minima.

Step 5: The algorithm is stopped if the current iteration I_t reaches the maximum iteration I_{max}, otherwise it goes back to step 2 to continue the search. The flowchart of the MNSGA-II is given in Fig. 2.

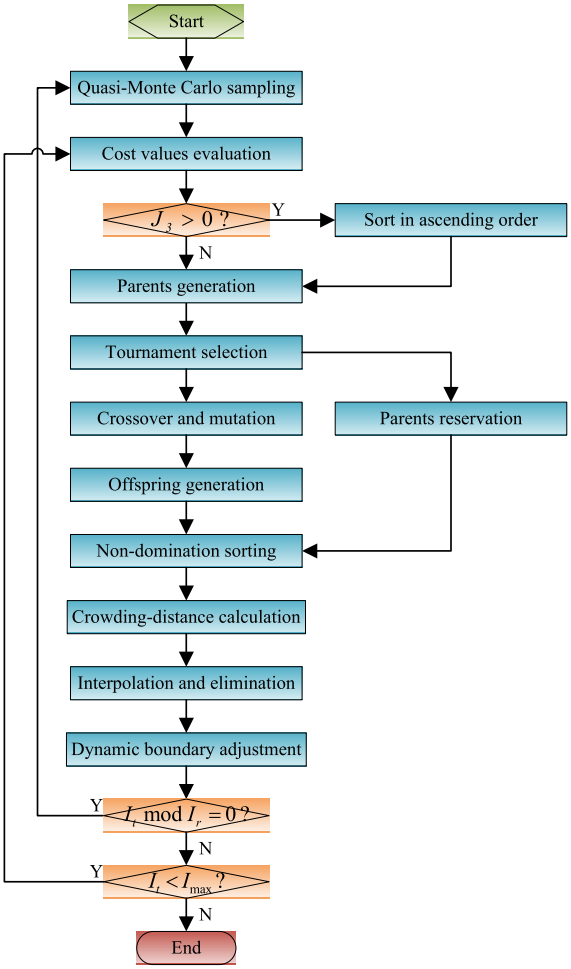

FIGURE 2. Flowchart of the MNSGA-II.

TABLE 3. Parameter settings of MNSGA-II.

Parameter	Value	Parameter	Value
N	100	I_r	200
D	12	I_{max}	1000
d_c	10	ω_i	1000
d_e	0.5	ω_e	100
L_0	50	ω_0	2.5

IV. SIMULATION AND EVALUATION

A. SIMULATION SETTINGS

To test the performance of the proposed algorithm, the MNSGA-II is compared with three other heuristic based multi-objective optimization algorithms: ISFLA [25], MOVPSO [26] and HNDS [27]. The parameter values of MNSGA-II are given in Table 3. As for ISFLA, MOVPSO and HNDS, the parameter settings are predefined in their corresponding references. All simulations are performed on a PC with Intel Core i7 processor of 3.4 GHz and 16GB of RAM.

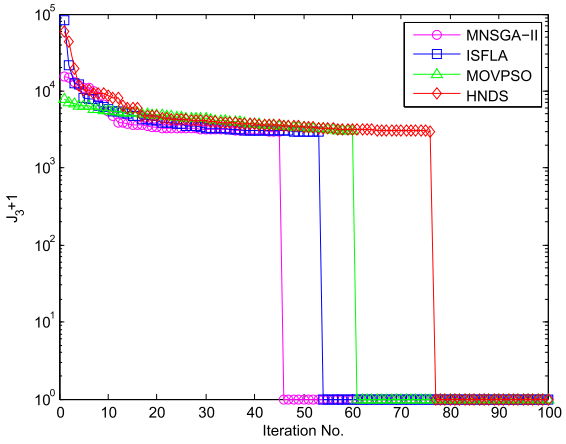

FIGURE 3. Convergence curves comparing MNSGA-II with 3 other heuristics based multi-objective optimization algorithms.

TABLE 4. Statistical data of the convergence curves.

Convergence step	MNSGA-II	ISFLA	MOVPSO	HNDS
Max. step	52	68	75	95
Average step	43	55	64	73
Min. step	36	47	54	58
Standard deviation	6.105	8.461	7.511	12.861

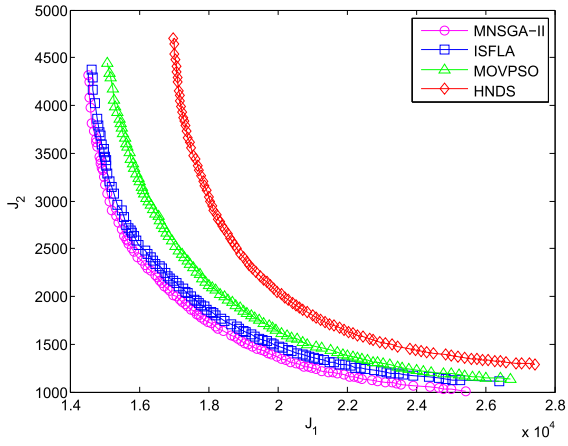

FIGURE 4. Control allocation relationship curves comparing MNSGA-II with 3 other heuristics based multi-objective optimization algorithms.

B. RESULTS ON THE COST VALUES

The convergence curves of the four algorithms under flying quality level 1 are presented in Fig. 3. All of the algorithms converge in the first 100 iterations with $J_3 = 0$, whereas both MNSGA-II and ISFLA show faster convergence speeds than the others. The simulations are carried out 30 times and statistical data of the convergence curves are given in Table 4. It can found that MNSGA-II and ISFLA still show better average convergence speeds than the others, whereas MNSGA-II works more stably with the lowest standard deviation.

Using the four algorithms, the control allocation relationship curves of the aileron and rudder channels under flying quality 1 are presented in Fig. 4. The cost value ranges of

TABLE 5. Statistical data of the convergence curves.

Cost value	MNSGA-II	ISFLA	MOVPSO	HNDS
Min. J_1	1.453×10^4	1.464×10^4	1.509×10^4	1.699×10^4
Max. J_1	2.543×10^4	2.639×10^4	2.672×10^4	2.743×10^4
Min. J_2	1.009×10^3	1.106×10^3	1.138×10^3	1.291×10^3
Max. J_2	4.310×10^3	4.377×10^3	4.448×10^3	4.697×10^3

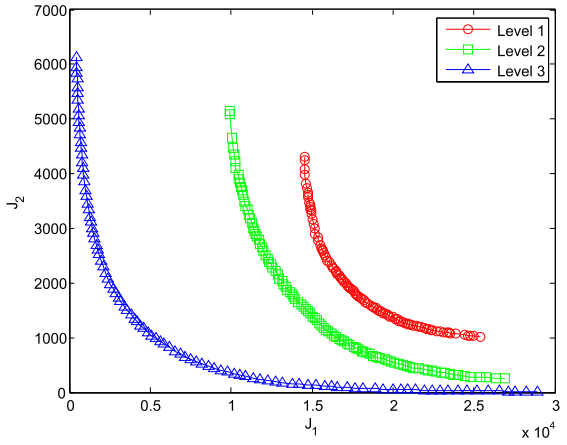

FIGURE 5. Control relationship curves on the three flying quality levels found using the MNSGA-II algorithm.

J_1 and J_2 are given in Table 5. Both Fig. 4 and Table 5 show that all solutions have smooth non-dominated curves, but the solutions found by MNSGA-II form a better frontier than the others.

C. RESULTS ON THE NON-DOMINATED SOLUTIONS

Using the proposed algorithm, the simulations are carried out under the three flying quality levels from 1 to 3. The control allocation relationship curves presented in Fig. 5 show that the looser the requirements, the wider the solution ranges, which demonstrates that the solutions under higher flying quality levels (looser) dominate those under lower levels (stricter). It can also be found that the maximum value of J_1 is larger than that of J_2, which demonstrates that the aileron control channel plays a dominant role in the lateral FCS for large transport aircraft.

In order to illustrate the changing trends of the control energy costs and the total state variable deviations under three flying qualities, two index functions, F_1 and F_2, are defined as follows:

$$\begin{cases} F_1 = \dfrac{1}{T}\int_0^T \omega_{f1}(\delta_{ail})^2 + \omega_{f2}(\delta_{rud})^2 dt \\ F_2 = \dfrac{1}{T}\int_0^T \omega_{f3}r^2 + \omega_{f4}p^2 + \omega_{f5}\phi^2 \\ \qquad + \omega_{f6}\psi^2 + \omega_{f7}y^2 + \omega_{f8}n_y^2 dt \end{cases} \tag{11}$$

where ω_{fi} $(i = 1, 2, ..., 8)$ are the corresponding weight factors, and in this case all are set to 1. Fig. 6 shows that with the aileron control energy increasing, the total control energy is increasing, whereas the total state variable deviation is decreasing in Fig. 7, which demonstrates that there is a balance between the control energy costs and aircraft flying qualities. Both Fig. 6 and Fig. 7 show that a more strict flying

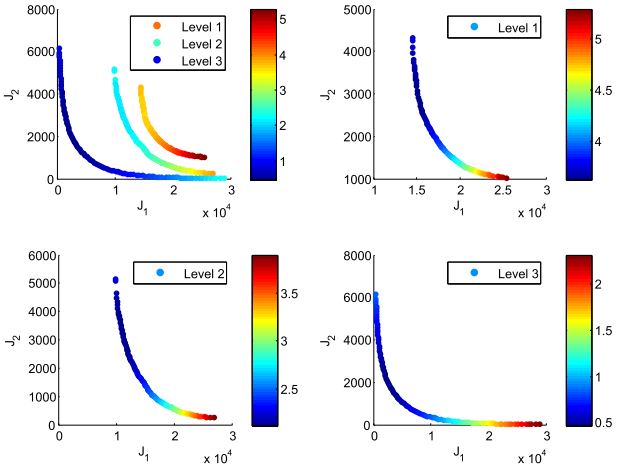

FIGURE 6. Changing trends of F_1 under the three flying qualities found using the MNSGA-II algorithm.

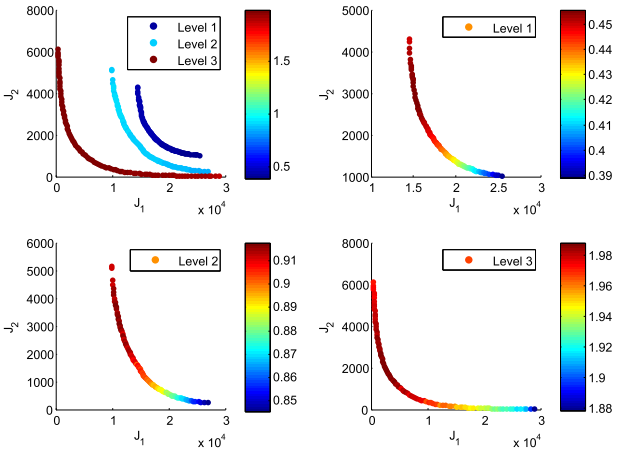

FIGURE 7. Changing trends of F_2 under the three flying qualities found using the MNSGA-II algorithm.

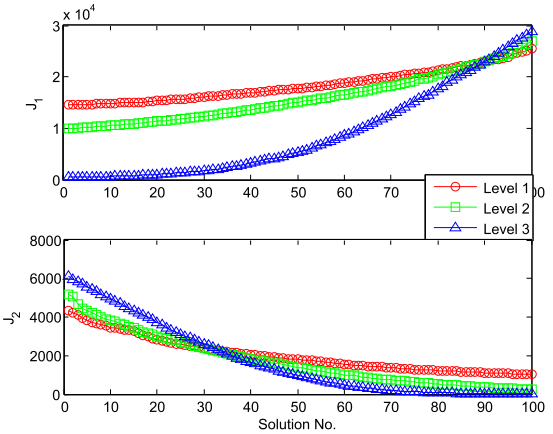

FIGURE 8. Energy costs of δ_{ail} and δ_{rud} for 3 different flying qualities found using the MNSGA-II algorithm.

quality level leads to an increase in control energy cost and a decrease in state variable deviation.

D. RESULTS ON THE STATE VARIABLES

Finally, the changing trends of the standard deviations of the six state variables are presented from Fig. 8 to Fig. 11,

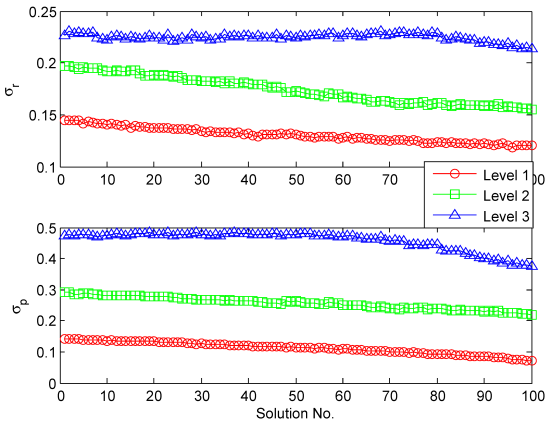

FIGURE 9. Standard deviations of r and p for 3 different flying qualities.

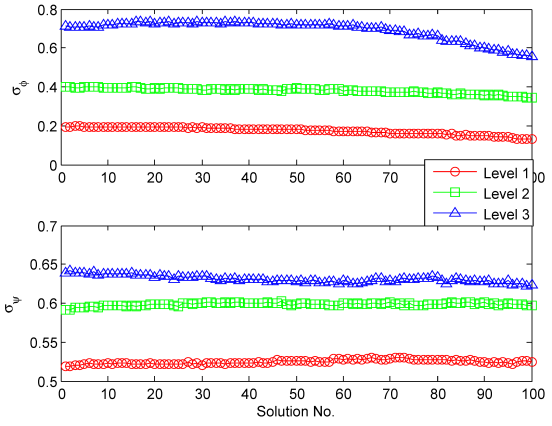

FIGURE 10. Standard deviations of ϕ and ψ for 3 different flying qualities.

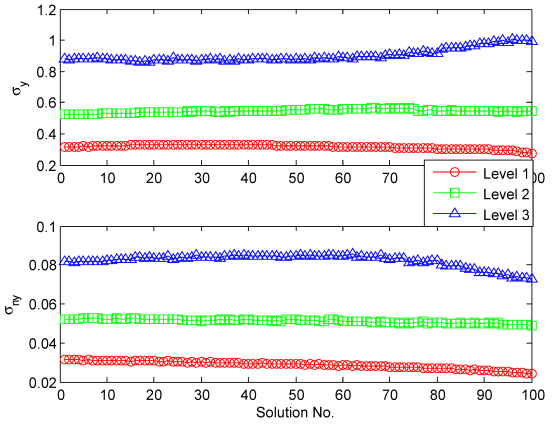

FIGURE 11. Standard deviations of y under n_y for 3 different flying qualities.

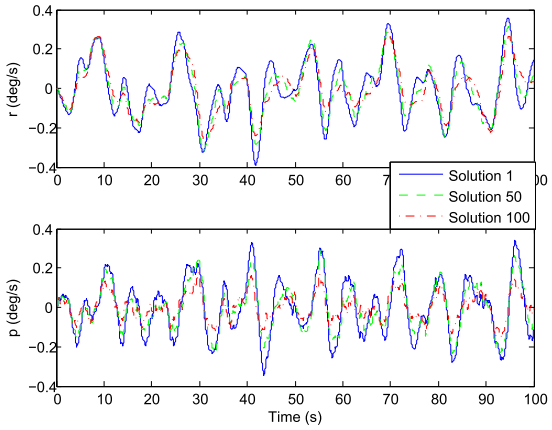

FIGURE 12. Deviations of r and p in crosswind for 3 different solutions found using the MNSGA-II algorithm.

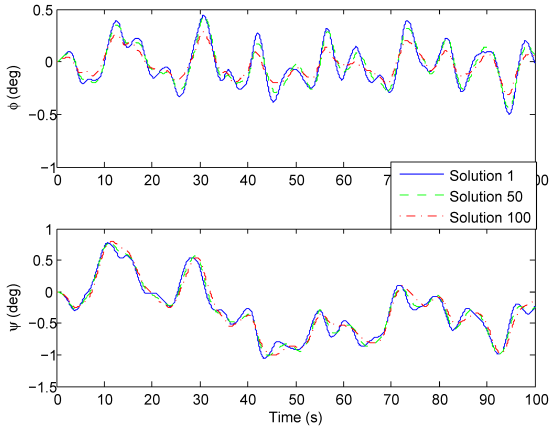

FIGURE 13. Deviations of ϕ and ψ in crosswind for 3 different solutions found using the MNSGA-II algorithm.

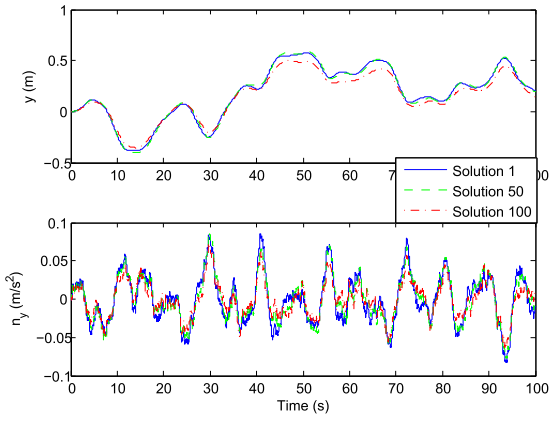

FIGURE 14. Deviations of y and n_y in crosswind for 3 different solutions found using the MNSGA-II algorithm.

respectively, where the 100 solutions refer to the corresponding 100 points on the relationship curves of J_1 and J_2. With a more strict flying quality level, the state variables become more stable with lower standard deviations. Besides, with the increasing control energy of the aileron channel, most of the state variables also become more stable, especially for the two angular rate signals, r and p.

In order to test the performance of the optimized FCS, three selected solutions (No. 1, 50 and 100) on the level 1 curve are tested. The control inputs and deviations of the six state-variables in 100 second simulations are given in Fig. 12 to Fig. 15. It can be found that all state variables are confined within the pre-defined limitations and the optimized

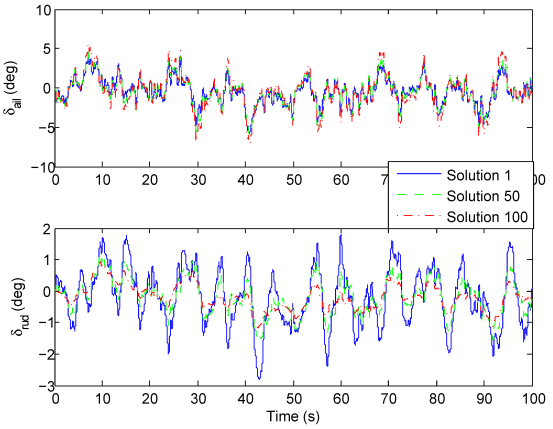

FIGURE 15. Control inputs of δ_{ail} and δ_{rud} for 3 different solutions found using the MNSGA-II algorithm.

FCS works stably over the whole process, which once again demonstrates the effectiveness of the proposed method.

V. CONCLUSION

In this paper, an effective MNSGA-II is developed to not only optimize the control allocations between the aileron and rudder channels with different flying qualities, but also to explore the relationships between the optimum solutions and the corresponding state variables of the aircraft. Crowding-distance based interpolation and elimination strategies combined with the dynamic deepening search method are developed to dynamically adjust the search domain and finally approach the optimum Pareto frontier. Comparative simulations of the proposed algorithm against three other multi-objective optimization algorithms demonstrate its feasibility and efficiency. It has been found that the aileron control channel plays a dominant role in the lateral FCS of large transport aircraft. Moreover, the control relationships between the aileron and rudder channels on different flying quality levels are also illustrated. The simulation results demonstrate that a more strict flying quality requirement can cause an increase in control energy cost, whereas the deviations of state variables are largely reduced. Since the control allocation relationships between the two channels have been explored, further research will focus on the high dimensional multi-objective optimization problems in a more complicated FCS.

DISCLOSURE STATEMENTS

The authors declare no conflict of interest.

REFERENCES

[1] Y. Zhao, C. Yue, and H. Hu, "Gust load alleviation on a large transport airplane," *J. Aircraft*, vol. 53, no. 6, pp. 1932–1946, 2016.

[2] C. Li, T. Zhang, and J. Yang, "Attitude control of aircraft using only synthetic jet actuators when stall occurs," *IEEE Access*, vol. 6, pp. 37910–37917, 2018.

[3] B. L. Stevens, F. L. Lewis, and E. N. Johnson, *Aircraft Control and Simulation: Dynamics, Controls Design, and Autonomous Systems*. Hoboken, NJ, USA: Wiley, 2015.

[4] Y. Liu, Z. Gao, and C. Shang, "Control allocation for an over-actuated aircraft based on within-visual-range air combat agility," *IEEE Access*, vol. 6, pp. 14668–14675, 2018.

[5] T. Guo, Z. Hou, and B. Zhu, "Dynamic modeling and active morphing trajectory-attitude separation control approach for gull-wing aircraft," *IEEE Access*, vol. 5, pp. 17006–17019, 2017.

[6] Q. Bian, K. Zhao, X. Wang, and R. Xie, "System identification method for small unmanned helicopter based on improved particle swarm optimization," *J. Bionic Eng.*, vol. 13, no. 3, pp. 504–514, 2016.

[7] B. S. Girish, "An efficient hybrid particle swarm optimization algorithm in a rolling horizon framework for the aircraft landing problem," *Appl. Soft Comput.*, vol. 44, pp. 200–221, Jul. 2016.

[8] A. G. Roy and N. K. Peyada, "Aircraft parameter estimation using hybrid neuro fuzzy and artificial bee colony optimization (HNFABC) algorithm," *Aerosp. Sci. Technol.*, vol. 71, pp. 772–782, Dec. 2017.

[9] Y. Marinakis, A. Migdalas, and A. Sifaleras, "A hybrid particle swarm optimization—Variable neighborhood search algorithm for constrained shortest path problems," *Eur. J. Oper. Res.*, vol. 261, no. 3, pp. 819–834, 2017.

[10] P. J. G. Nieto, E. García-Gonzalo, F. S. Lasheras, and F. J. de Cos Juez, "Hybrid PSO–SVM-based method for forecasting of the remaining useful life for aircraft engines and evaluation of its reliability," *Rel. Eng. Syst. Saf.*, vol. 138, pp. 219–231, Jun. 2015.

[11] Y. Deng and H. Duan, "Control parameter design for automatic carrier landing system via pigeon-inspired optimization," *Nonlinear Dyn.*, vol. 85, no. 1, pp. 97–106, 2016.

[12] R. Dou and H. Duan, "Lévy flight based pigeon-inspired optimization for control parameters optimization in automatic carrier landing system," *Aerosp. Sci. Technol.*, vol. 61, pp. 11–20, Feb. 2017.

[13] C. R. Hanke, "The simulation of a large jet transport aircraft. Volume 1—-Mathematical model," Boeing Company, Chicago, IL, USA, Tech. Rep. NASA CR-1756, 1971.

[14] C. R. Hanke and D. R. Nordwall, "The simulation of a jumbo jet transport aircraft. Volume 2: Modeling data," Boeing Company, Chicago, IL, USA, Tech. Rep., D6 -30643, 1970.

[15] J. Roskam, *Airplane Flight Dynamics and Automatic Flight Controls*. Lawrence, KS, USA: Design, Analysis and Research Corporation, 2001.

[16] F. M. Hoblit, *Gust Loads on Aircraft: Concepts and Applications*. Washington, DC, USA: The American Institute of Aeronautics and Astronautics, 1988.

[17] M. Lungu and R. Lungu, "Automatic control of aircraft lateral-directional motion during landing using neural networks and radio-technical subsystems," *Neurocomputing*, vol. 171, pp. 471–481, Jan. 2016.

[18] M. Lungu and R. Lungu, "Neural network based adaptive control of airplane's lateral-directional motion during final approach phase of landing," *Eng. Appl. Artif. Intell.*, vol. 74, pp. 322–335, Sep. 2018.

[19] *Flying Qualities of Piloted Aircraft*, Standard MIL-HDBK-1797, Handbook, FSC 15GP, Department of Defense, Washington, DC, USA, 1997.

[20] C. K. H. Lee, "A review of applications of genetic algorithms in operations management," *Eng. Appl. Artif. Intell.*, vol. 76, pp. 1–12, Nov. 2018.

[21] T. Bhoskar, O. K. Kulkarni, N. K. Kulkarni, S. L. Patekar, G. M. Kakandikar, and V. M. Nandedkar, "Genetic algorithm and its applications to mechanical engineering: A review," *Mater. Today, Proc.*, vol. 2, nos. 4–5, pp. 2624–2630, 2015.

[22] T. Goda, "Quasi-Monte Carlo integration using digital nets with antithetics," *J. Comput. Appl. Math.*, vol. 304, pp. 26–42, Oct. 2016.

[23] K. Deb, A. Pratap, S. Agarwal, and T. Meyarivan, "A fast and elitist multiobjective genetic algorithm: NSGA-II," *IEEE Trans. Evol. Comput.*, vol. 6, no. 2, pp. 182–197, Apr. 2002.

[24] Q. Bian, B. Nener, and X. Wang, "An improved NSGA-II based control allocation optimisation for aircraft longitudinal automatic landing system," *Int. J. Control*, May 2018, pp. 1–12. doi: 10.1080/00207179.2018.1473643.

[25] J. Luo, Y. Yang, Q. Liu, X. Li, M. Chen, and K. Gao, "A new hybrid memetic multi-objective optimization algorithm for multi-objective optimization," *Inf. Sci.*, vol. 448, pp. 164–186, Jun. 2018.

[26] J. Meza, H. Espitia, C. Montenegro, E. Giménez, R. González-Crespo, "MOVPSO: Vortex multi-objective particle swarm optimization," *Appl. Soft Comput.*, vol. 52, pp. 1042–1057, Mar. 2017.

[27] C. Bao, L. Xu, Goodman, E. D. Goodman, and L. Cao, "A novel non-dominated sorting algorithm for evolutionary multi-objective optimization," *J. Comput. Sci.*, vol. 23, pp. 31–43, Nov. 2017.

QI BIAN received the B.S. and M.S. degrees in control theories and applications from Northwestern Polytechnical University, Xi'an, China, where he is currently pursuing the Ph.D. degree. His research interests include control and optimization.

BRETT NENER received the B.E. and Ph.D. degrees from the University of Western Australia, and the M.Sc. degree from the University of Tokyo. He has been a Visiting Professor with the U.S. Navy Space and Naval Warfare Center, San Diego, CA, USA, the University of California at Santa Barbara, and the Japanese National Institute of Information and Communications Technology. He is currently a Professor with the Department of Electrical, Electronic and Computer Engineering, The University of Western Australia, where he was the Head of the Department from 2008 to 2014.

XINMIN WANG received the B.S. from Northwestern Polytechnical University, and the M.S. degree from the Nanjing University of Science and Technology. In 1976, he joined the School of Automation, Northwestern Polytechnical University, where he is currently a Professor. His research interests include flight control and simulation technology, and advanced control theory and applications.